1 Introduction

Solar collectors are heat exchangers designed to convert incident solar radiation into thermal energy for practical applications. Unlike conventional heat exchangers that facilitate fluid-to-fluid heat transfer, solar collectors capture radiant energy from the sun and transfer it to a working fluid through an absorber surface. While solar collectors lack the operational flexibility of traditional heat exchangers in terms of sizing, placement, and maintenance scheduling, they offer significant advantages including zero fuel costs after installation and no greenhouse gas emissions during operation.[1]

The fundamental challenge in solar collector design stems from the variable and relatively low-intensity nature of solar radiation. Solar irradiance varies diurnally from 0 to 1000 W/m^2 and seasonally due to sun angle variations, while conventional heat sources provide steady, high-intensity thermal input. This variability necessitates optimization of the absorber surface to maximize solar energy capture while minimizing thermal losses. Effective solar collectors must selectively absorb short-wavelength solar radiation (0.3-3 µm) while suppressing emission of long-wavelength thermal radiation (3-50 µm) that increases with surface temperature.[2]

Collector thermal performance is fundamentally governed by the energy balance between solar gains and thermal losses to the environment. Heat loss mechanisms include conduction through the collector structure, convection to ambient air, and radiation from the heated absorber surface. The resulting temperature-dependent efficiency requires careful matching of collector design to application requirements, with low-temperature applications (pool heating) achieving 70-80% efficiency while higher-temperature processes (space heating) operate at 40-60% efficiency.[3]

Flat-plate collectors dominate the residential and commercial market due to their ability to utilize both direct and diffuse radiation without sun-tracking mechanisms. These systems consist of a blackened absorber plate with integrated fluid passages, transparent glazing to reduce convective losses, and thermal insulation within a weather-resistant enclosure. The thermal analysis of flat-plate collectors involves complex coupled heat transfer processes, though simplified design equations enable practical performance calculations for system optimization and economic analysis.

2 Theory

Flat-plate solar collectors convert incident solar radiation into thermal energy through a complex heat transfer process involving absorption, conduction, and convection. The collector's thermal performance is characterized by two fundamental parameters: steady-state efficiency and dynamic thermal response. Understanding both characteristics is essential for system design and control applications.

Under steady-state conditions, the useful energy gain rate from a solar collector is governed by the energy balance,

$$Q_u = A_c[S - U_L(T_{pm} - T_a)] \tag{1}$$

where Q_u is the useful heat gain rate (W), A_c is the collector aperture area (m^2), S is the absorbed solar radiation per unit area (W/m^2), U_L is the overall heat loss coefficient (W/m^2·K), T_{pm} is the mean absorber plate temperature (°C), and T_a is the ambient temperature (°C). The absorbed solar radiation $S = (\tau\alpha)G_T$ represents the product of the optical efficiency $(\tau\alpha)$ and incident irradiance G_T (W/m^2).

Since direct measurement of the mean plate temperature is impractical, collector efficiency is expressed in terms of measurable fluid temperatures. The instantaneous thermal efficiency is defined as

$$\eta = \frac{Q_u}{A_c G_T} = \frac{\dot{m} c_p (T_o - T_i)}{A_c G_T} \tag{2}$$

where $\dot{m}$ is the mass flow rate (kg/s), c_p is the fluid specific heat capacity (J/kg·K), and T_i and T_o are the inlet and outlet fluid temperatures (°C), respectively. This definition quantifies the fraction of incident solar energy successfully transferred to the working fluid.

For performance characterization and comparison with manufacturer data, the efficiency relationship is linearized by relating collector performance to operating conditions. Through heat transfer analysis, the efficiency can be expressed as

$$\eta = F_R(\tau\alpha) - F_R U_L \frac{(T_i - T_a)}{G_T} \tag{3}$$

where F_R is the heat removal factor (dimensionless) that accounts for the temperature rise of fluid flowing through the collector. The term $F_R(\tau\alpha)$ represents the optical efficiency intercept—the theoretical efficiency when inlet temperature equals ambient temperature. The slope $F_R U_L$ characterizes thermal losses, with larger values indicating greater sensitivity to elevated operating temperatures. This linear relationship enables direct comparison between experimental measurements and certified performance curves by plotting efficiency versus the reduced temperature parameter $(T_i - T_a)/G_T$.

The collector's dynamic thermal response is characterized by its ability to reach new steady-state conditions following disturbances in operating parameters. For systems with significant thermal mass, the transient response to a step change in inlet temperature follows first-order dynamics:

$$T_o(t) = T_{o,\infty} + [T_{o,0} - T_{o,\infty}]e^{-t/\tau} \tag{4}$$

where $T_{o,0}$ is the initial outlet temperature, $T_{o,\infty}$ is the final steady-state outlet temperature, and τ is the thermal time constant (s). The time constant represents the time required for the outlet temperature to reach 63.2% of its total change toward the new equilibrium value.

The thermal time constant depends on the system's thermal capacitance and the rate of heat removal

$$\tau = \frac{(MC_p)_{effective}}{\dot{m}c_p + A_c U_L} \tag{5}$$

where $(MC_p)_{effective}$ represents the effective thermal capacitance of the collector system, including the absorber plate, fluid inventory, piping, and glazing components. The denominator represents the total thermal conductance, comprising both convective heat removal by the fluid and conductive/radiative losses to the environment. A shorter time constant indicates rapid thermal response but may also suggest reduced thermal mass or higher heat loss rates.

Experimental determination of the time constant involves creating a step change in system boundary conditions and monitoring the exponential approach to equilibrium. In this study, the time constant is measured by implementing a step change in inlet fluid temperature while maintaining constant irradiance and flow rate. The resulting outlet temperature response provides direct measurement of the collector's thermal inertia, which is critical for understanding system behavior under variable operating conditions and for designing appropriate control strategies.

The relationship between flow rate and collector performance is particularly important for understanding deviations from standard test conditions. Reduced flow rates increase fluid residence time within the collector, leading to higher outlet temperatures but potentially reducing the heat removal factor F_R. This flow-rate dependency affects both the optical efficiency intercept and thermal loss coefficient in the linearized performance equation, making flow rate a critical parameter for accurate performance characterization.[3]

3 Methods

3.1 Experimental Setup

The experimental apparatus consisted of a ThermoRay TRB-26 flat-plate solar collector integrated into a two-tank water circulation system (inlet tank at a constant temperature). The collector was oriented to face the equator and tilted at 36.3° from horizontal to optimize solar irradiance capture for the test location (32.7° N, San Diego, CA). A constant mass flow rate of 0.031 kg/s was maintained throughout all experiments using a calibrated centrifugal pump with flow control valve.

Temperature measurements were acquired using Type-T thermocouples connected to an Arduino-based data acquisition system. Inlet temperature (T_i) and outlet temperature (T_o) were measured at the collector fluid connections. Solar irradiance (G_T) was measured using a pyranometer mounted coplanar with the collector surface. All sensors were logged at 1-second intervals with measurement uncertainties of ±2.22°C [4] for temperature, ±1.00% [5] for irradiance and 1.30% [6] for flow rate measurements.

3.2 Steady-State Efficiency Characterization

Collector efficiency was determined under steady-state conditions by establishing thermal equilibrium at various inlet fluid temperatures. For each test point, the system was operated until inlet, outlet, and ambient temperatures remained constant. Steady-state was defined as temperature variations less than 0.5°C over a 30-second period.

Instantaneous efficiency was calculated using Equation 2 with fluid properties evaluated at the mean temperature. Multiple data points were collected by varying the inlet temperature through adjustment of an upstream heat exchanger, creating a range of reduced temperature parameters $(T_i - T_a)/G_T$ from approximately 0.002 to 0.012 $m^2 \cdot K/W$. Natural solar irradiance was utilized when possible, supplemented by artificial illumination using an array of 11 halogen lamps to maintain consistent test conditions during periods of variable cloud cover.

The linearized efficiency relationship (Equation 3) was fitted to experimental data using least-squares linear regression. Statistical significance of the correlation was assessed using F-test analysis with $\alpha = 0.05$ significance level. The optical efficiency intercept $F_R(\tau\alpha)$ and thermal loss slope $F_R U_L$ were extracted from the regression parameters and compared with manufacturer certified values of 0.740 and 4.115 $W/m^2 \cdot K$, respectively.

3.3 Thermal Time Constant Measurement

Dynamic thermal response was characterized by measuring the collector's time constant following a step change in inlet fluid temperature. The system was first established at steady-state conditions with inlet temperature significantly above ambient temperature. A step reduction in inlet temperature was then implemented by rapidly switching the fluid supply to an ambient-temperature reservoir while maintaining constant flow rate and solar irradiance.

Outlet temperature response was continuously recorded during the subsequent transient period until a new steady-state was achieved. The thermal time constant was determined by fitting the exponential decay function (Equation 4) to the experimental data using nonlinear regression. Due to inlet temperature fluctuations of ± 1°C during the measurement period, the average inlet temperature of 28.75°C was used as the reference value rather than the instantaneous temperature at $t = 0$.

The effective thermal capacitance was calculated from the measured time constant using Equation 5, with fluid properties evaluated at operating temperature and collector heat loss coefficient estimated from steady-state efficiency measurements. Uncertainty in the time constant was propagated through the calculation to determine confidence intervals for the thermal capacitance estimate.

3.4 Uncertainty Analysis

Measurement uncertainties were determined from instrument specifications and calibration data. Temperature measurements carried an uncertainty of ±2.22°C [4] based on thermocouple accuracy and data acquisition resolution. Mass flow rate uncertainty was estimated at 1.30% [6] from flow meter specifications. Solar irradiance measurements were accurate to ±1.00% [5] according to pyranometer calibration certificates.

Propagation of uncertainties through calculated quantities was performed using standard methods for uncorrelated random variables. For efficiency calculations, the dominant uncertainty sources were temperature difference measurements and irradiance readings.

3.5 Data Analysis

All data processing and statistical analysis were performed using standard computational methods. Linear regression analysis included calculation of correlation coefficient, and significance testing. The coefficient of determination (R^2) was used to assess goodness of fit, while F-statistics were compared against critical values to establish statistical significance of observed correlations. Experimental results were systematically compared with manufacturer performance data to quantify deviations and identify potential sources of discrepancy.

4 Results and Discussion

The ThermoRay TRB-26 collector exhibited rapid thermal dynamics during transient testing, reaching equilibrium in just 2.13 ± 0.17 minutes following solar input cessation. This time constant of $\tau = 127.5 \pm 10.1$ s corresponds to an effective thermal capacitance of only 1,773 J/K—substantially lower than the theoretical estimate of 14,182 J/K for typical collector construction. Such minimal thermal inertia proves advantageous for systems experiencing variable cloud cover but raises questions about the collector's actual construction or potential measurement artifacts. This is shown in 1. The average of inlet temperature is considered instead of the inlet temperature at $t = 0$ min as 28.75(44) °C due to ± 1 °C fluctuation at times. Steady-state efficiency testing revealed significant performance shortfalls compared to manufacturer specifications. The experimental data yielded a linear efficiency relationship with optical intercept $\mathrm{F}_R(\tau\alpha)_n = 0.378(34)$ and thermal loss

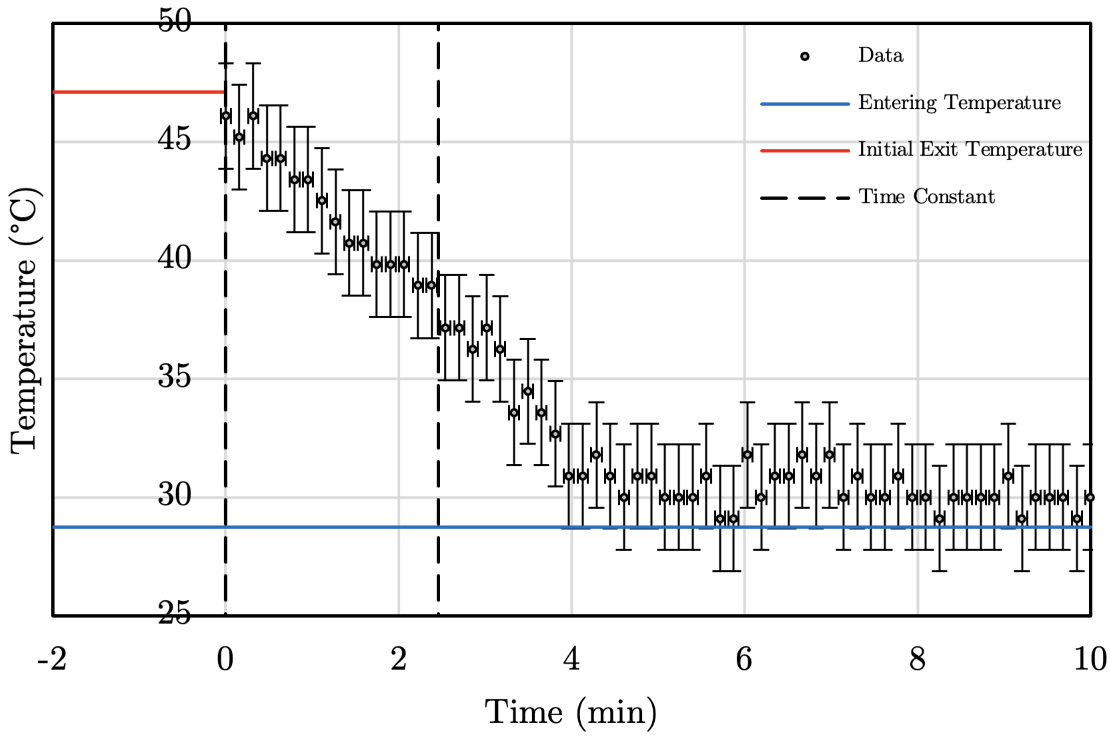

Figure 1: Thermal time constant measurement showing exponential temperature decay following step change in inlet temperature at t = 0. The outlet temperature is represented with black data points with error bars. Time constant is 2.13 minutes. Error bars represent ±2.22 °C measurement uncertainty.

slope $F_R U_L$ = 1.97(44) W/m²·K. These values represent a 39.7% reduction in optical efficiency and 35.5% increase in thermal losses relative to the certified values of 0.740 and 4.115 W/m²·K, respectively.

The elevated thermal losses trace directly to sub-optimal flow conditions during testing. Operating at 0.031 kg/s instead of the standard 0.050 kg/s $(0.020\,\mathrm{kg/(s \cdot m^2)})$[7]—a 37.9% reduction—altered the collector's thermal behavior. This reduced flow forced the working fluid to undergo a temperature rise of 7.7°C across the collector compared to only 4.8°C at standard flow, resulting in an additional 2.9°C temperature elevation. In other words, the temperature differential between the moving fluid and the plate itself is smaller, making the transfer of heat from the plate into the moving fluid slower. Hence the plate cools less quickly than it would running at 0.050 kg/s. The overall temperature of exiting fluid is still higher.

The coefficient of determination $R^2 = 0.835$ indicates linear correlation between efficiency and temperature differential. The regression is statistically significant (F-statistic = 20.3 > F-critical =

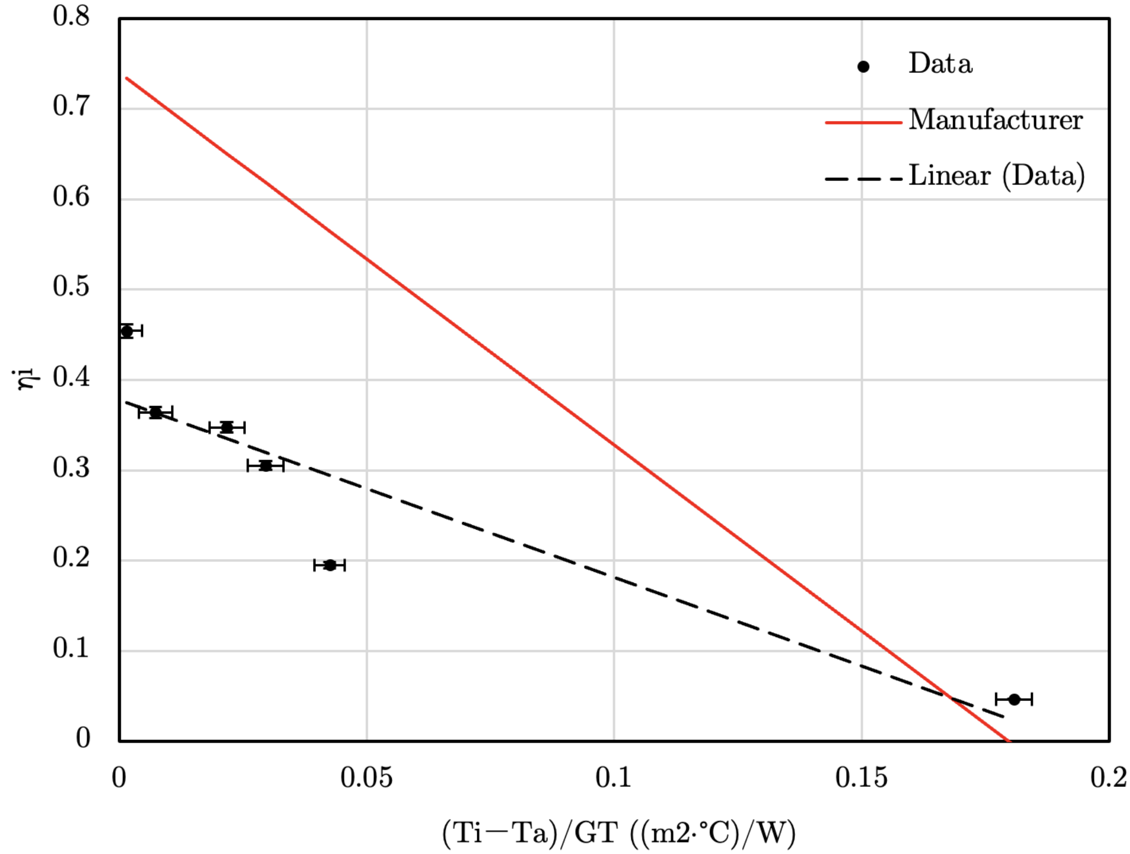

Figure 2: Collector efficiency curve comparing experimental measurements with manufacturer specifications. Experimental data points (black circles) with error bars show instantaneous efficiency versus the normalized temperature difference. The dashed black line represents the linear regression fit.

7.71), confirming the linear relationship is not due to random chance. The data however does not fairly capture an equally spaced amounts of $(T_i - T_a)/G_T$, across the x-axis. Even though there is an average of 9.7 °C between each of the inlet temperatures across each trial, this was still difficult to achieve due to an average increase of 12.8 % irradiance when capturing energy from natural light as opposed to using lamps. What should have been done instead is to not space out the inlet temperatures but rather equally space out $(T_i - T_a)/G_T$ to better represent the regression fit.

5 Conclusion

Experimental characterization of the ThermoRay TRB-26 solar collector revealed significant performance deviations from manufacturer specifications under non-standard operating conditions. The measured optical efficiency intercept of 0.378 represents a 39.7% reduction from the certified value of 0.740, while thermal losses increased by 35.5% compared to manufacturer data. These discrepancies are primarily attributed to sub-optimal flow conditions, with the experimental flow rate of 0.031 kg/s being 37.9% below the standard test condition of 0.050 kg/s.

The collector exhibited rapid thermal response characteristics with a time constant of 2.13 ± 0.17 minutes, corresponding to an effective thermal capacitance of only 1,773 J/K. This minimal thermal inertia indicates either lightweight construction or potential measurement artifacts, but proves advantageous for applications experiencing variable solar conditions.

The strong linear correlation between efficiency and reduced temperature parameter (R^2 = 0.835) confirms the validity of the standard collector performance model under the tested conditions. However, the substantial performance degradation at reduced flow rates demonstrates the critical importance of maintaining design operating conditions for achieving rated collector performance in practical solar thermal systems.

References

(1) Kalogirou, S. A., *Solar Energy Engineering: Processes and Systems*, 2nd; Academic Press: Amsterdam, 2014.

(2) Duffie, J. A.; Beckman, W. A.; Blair, N., *Solar Engineering of Thermal Processes, Photovoltaics and Wind*, 5th; John Wiley & Sons: Hoboken, NJ, 2020.

(3) Tian, M.; Su, Y.; Zheng, H.; Pei, G.; Li, G.; Riffat, S. *Renewable and Sustainable Energy Reviews* **2018**, *82*, 1272–1296.

(4) McMaster-Carr High-Temperature High-Strength Grade 5 Titanium (Ti-6Al-4V) Rods and Discs, Online Catalog, Accessed on June 11, 2025. Part No. 3856K912, 2025.

(5) Vernier Software & Technology Pyranometer (PYR-BTA), Revision 9/18/2012; Vernier Software & Technology, Beaverton, OR, 2012.

(6) P3 International Corporation Save A Drop™ Water Meter Operation Manual, Model P0550, Revision 0518; P3 International Corporation, 2018.

(7) Duffie, J. A.; Beckman, W. A., *Solar Engineering of Thermal Processes*, 5th; John Wiley & Sons: 2020.

Appendix A

Table 1: Uncertainties of measured quantities.

Description	**Variable**	**Unc.**	**Unit**
mass flow rate	m	1.30%	kg/s
temperature	T_i, T_o, T_a	2.22	°C
irradiance	G_T	1.00%	W/m^2

Table 2: Source data for linearized efficiency plot.

Light source	m **(kg/s)**	T_i **(°C)**	T_o **(°C)**	T_a **(°C)**	G_T **(W/m^2)**	**num. lights**
Sun	0.031511183	31.51013611	37.9477488	24.7	934.574604	
Sun	0.033228667	25.74452747	34.0368571	24.2	1016.81646	
Lamps	0.0299058	38.15336017	44.2929597	18.9	886.914	11
Lamps	0.0297066	44.69778749	50.1291677	18.5	886.914	11
Sun	0.031012433	68.3283	72.1371428	25.2	1015.7458	
Sun	0.031012433	68.6889712	72.1855291	21.8	1006.20031	